Subsidence Characteristics Study on the Highway and Substrata Overlying Acute Inclined Shallow Mined-out Area Under Different Mining Heights and Mining Angles

Weixing Bao
Chang'an University
Haibo Wang
Chang'an University
Hongpeng Lai (laihp168@chd.edu.cn)
Chang'an University
Zifeng Zhao
CCCC FIRST HIGHWAY CONSULTANTS Co Ltd
Bangwei Liang
CCCC SECOND HARBOUR ENGINEERING COMPANY LTD
Yong Huang
XINJIANG COMMUNICATIONS CONSTRUCTION GROUP CO., LTD
Zhiwei Ma
Chang'an University

Research Article

Keywords: Mined-out area, Physical model experiment, Finite difference analysis, Mining-induced subsidence, Acute inclined mine seam

Posted Date: June 25th, 2021

DOI: https://doi.org/10.21203/rs.3.rs-562034/v1

Subsidence Characteristics Study on the Highway and Substrata Overlying Acute Inclined Shallow Mined-out Area Under Different Mining Heights and Mining Angles

Weixing Bao[1], Haibo Wang[1], Hongpeng Lai[1*], Zifeng Zhao[2], Bangwei Liang [3], Yong Huang [4], Zhiwei Ma[1]

[1] School of Highway, Chang'an University, Xi'an, 710064, Shaanxi Province, China

[2] CCCC FIRST HIGHWAY CONSULTANTS CO.,LTD, Xi'an, 710075, Shaanxi Province, China

[3] CCCC SECOND HARBOUR ENGINEERING COMPANY LTD. Wuhan, 430040, Hubei Province, China

[4] XINJIANG COMMUNICATIONS CONSTRUCTION GROUP CO.,LTD. Urumqi, 830026, the Xinjiang Uygur Autonomous Region, China

*Corresponding author: Hongpeng Lai; E-mail address: laihp168@chd.edu.cn

Abstract: Based on an actual highway project traversing an acute inclined shallow mined-out area in Urumqi, China, a scale physical model experiment and numerical simulation method were adopted to study the stability and settlement mechanism of the highway subgrade and substrata overlying an acute inclined mined-out area under different mining heights and mining angles. Plastic pneumatic capsules with different shapes were embedded in similar strata made from clay, fine sand, and Vaseline to simulate the mined-out cavity. The capsule was removed to simulate the process of mining, and five cases with different mining heights and angles were studied. According to similarity theory, a physical model was established with a geometric similarity coefficient of 50 of the actual prototype, whereas the numerical model adopted the full-scale value. The physical model experiments and numerical simulations show that the settlement of the subgrade and substrata overlying the mined-out area is directly proportional to the mining height but inversely proportional to the mining angle. According to

the settlement contour obtained by numerical simulations, which were in accordance with the physical model experiment results, two parameters, the free slip volume and the free surface, were defined to assess the stability of the subgrade and substrata overlying the mined-out area. The free slip volume and free surface calculation results demonstrate a strong relationship between the settlement and free slip volume and free surface. Therefore, the values of free slip volume and free surface could be reliable reference parameters to evaluate the stability of the subgrade and substrata overlying mined-out areas.

Keywords: Mined-out area; Physical model experiment; Finite difference analysis; Mining-induced subsidence; Acute inclined mine seam

Introduction

The ground movements and deformations resulting from underground mining activity can cause considerable damage to surface buildings, underground pipelines, and aquifers (Álvarez-Vigil et al., 2010; Bell and de Bruyn, 1999). Consequently, the settlement prediction and stability evaluation of mined-out areas are critical in assessing the likely damage potential to the environment and surface structures. With the need for economic development and highway network construction in many regions, highways traversing all kinds of mined-out areas are inevitable (Bao et al., 2021). The highway is a kind of long strip of civil engineering. There were many adverse effects on highway stability when traversing mined-out areas. The excavation damage zone and subsidence due to underground mines must be assessed and predicted as accurately as possible to maintain the subgrade's stability in the mined-out area.

The settlement mechanism and stability of the mined-out area are complex and affected by various factors. It is impossible and difficult to involve all factors in a study, there are numerous types of mined-out areas, and their stability features are always different. These factors include rock discontinuities (Cheng et al., 2018; O'Connor and Dowding, 1992), coal seam dip angle (Cui et al., 2013; Fang et al., 2016; Yao et al., 2017), topography (Fathi Salmi et al., 2017; Holla, 1997), mining depth (Xia et al., 2018), time (Salmi et al., 2017), number of mine seams (Ghabraie et al., 2017; Sui et al., 2015), landforms (Zhou et al., 2016), and mining speed (Xu et al., 2019). The dip angle is the prominent feature of acute inclined mined-out areas. Thus, the mining angle and mining height are chosen as the focus factors studied in this paper.

Empirical, physical model experiments, and analytical methods are the three primary approaches involved in the study of mining-induced subsidence (Zhou et al., 2016). The empirical approach is based on statistical solutions using ground movement measurement data to construct the displacement field (Marino et al., 2017). Physical model experiments establish simplified physical models to simulate actual engineering and geotechnical phenomena. Widely used analytical methods include numerical modeling methods (Fathi Salmi et al., 2017; Sepehri et al., 2017), probability integration methods (Zhang et al., 2016), graphical methods, profile function methods, influence function methods, and closed-form solutions (Huayang et al., 2010). Novel approaches were proposed based on the basic geotechnical theory; Sun et al. (2019a) proposed the Analogous Hyperbola Subsidence Model to describe the movement and damage of overburden during hallow coal seam mining based on key stratum theory and the mechanical analysis of overburden; Sun et al. (2019b) developed a feasible method for determining the movement of overburden caused by shallow coal mining based on the key stratum theory and Mohr-Coulomb failure criteria involving the formation of overburden; Guo et al.

(2019) established mechanical models of the unsupported strata and the overhanging strata based on rock failure criteria to predict the height of the fractured zone due to coal mining.

These methods are always frequently adopted in combination to increase the accuracy and reliability of the study and ensure the safe serviceability of the structures in mined-out areas. For instance, Sheorey et al. (2000) developed a modified influence function method for complete subsidence prediction based on ground subsidence observations in India's different coalfields. Based on field observations and numerical simulations, Meng et al. (2016) analyzed the characteristics of deformation, failure, and permeability of coal-bearing strata due to mining activities. Nie et al. (2017) adopted an arctangent function model combined with field monitoring subsidence data to predict ground mining subsidence. Huayang et al. (2010) carried out a scale model experiment to verify the accuracy of software for predicting the displacement and deformation of ground due to underground mining based on probability integration theory. Wang et al. (2017) studied the caving characteristics of overlying strata using both physical experiments on similar materials and numerical simulations of particle flow code (PFC) software and verified each other. According to the characteristics of the background engineering studied and the experimental conditions, physical model experiments and numerical simulations are chosen as the primary study methodologies in this paper.

For the convenience of mined-out area stability evaluation and strengthening works, the strata above the mined-out area were divided into shattered, fracture, and curvature zones based on the strata's deformation and integrity in China (Zhang and Wang, 2014). Xia et al. (2016) divided the mining-induced ground movement area into a toppling-sliding zone, a toppling zone, and a stability zone according to the monitoring data analysis for horizontal and vertical displacements over eight years of an iron mine. Cheng et al. (2017) divided the goaf surface deformation area into four zones:

the fracture extension zone, the fracture closure zone, the fracture formation zone, and the deformation accumulation zone based on the surface deformation characteristics analysis of an iron mine.

In this paper, based on an actual highway project traversing an acute inclined shallow mined-out area, a scale physical model and numerical model were built to study the stability and settlement mechanism of the subgrade and substrata overlying an acute inclined shallow mined-out area under different mining heights and mining angles. Settlement monitoring devices were embedded in the model box to monitor the settlement of the subgrade and substrata. The stability of the strata overlying mined-out space is affected by many factors. In this study, the mining height and mining angle were the main factors to explore. Thus, there were five experimental cases with different mining heights and angles in both the physical model experiment and numerical simulation.

Background

The Xinjiang Uygur Autonomous Region is the largest coal reserve region of China. Coal mining activity resulted in extensive mined-out areas in Xinjiang (Wang et al., 2005), and due to the dense population and infrastructures, its capital, Urumchi, surfers from more severe mined-out area problems. The east belt expressway of Urumchi was chosen as the background project of this study, which is approximately 62.5 km in length, and the width of the subgrade is 33.5 m. Many mines were surrounding the project, and the adverse settlement problem was plentiful. The line of the expressway traversed the Shagou Xinfu coal mine (330 m), Zhingxin No. 2 coal mine (660 m), Shuguang No. 6 coal mine (320 m), and Zhiqiang mine (300 m) from north to south successively. The coal-bearing strata are the Jurassic Xishanyao Formation and Badaowan Formation, with a total of 32 coal layers. The thickness of a single coal seam is approximately 0.7 m to 65 m, the buried depth of the coal seam

is approximately 15 m to 100 m, the strike is approximately 65° to 70°, and the dip angle is approximately 67° to 86°. Therefore, the mined-out areas in this region were acutely inclined shallow mined-out areas.

According to the detailed geological investigation results of the mined-out area along the route, the Shuguang No. 6 section was selected as the research object and prototype of the physical model experiment and numerical simulation. The longitudinal cross-section diagram of the Shuguang No. 6 mine along the route is shown in Fig. 1.

Scale Model Experiment

A large physical model box was adopted to simulate the mining process and pave the subgrade above the mined-out area. The model box was filled with similar material. Pneumatic capsule and settlement monitoring devices were embedded when filling the model box. The mining process was simulated by removing the pneumatic capsule from the filled model box.

The general process flowchart of a single experimental case is presented in Fig. 2.

Experiment Case Design

In this study, five experiments considered two factors (mining height and mining angle), and each factor was studied with three levels to examine the stability and settlement principle of highway subgrade overlying mined-out areas. The basic parameters of the five experiments were designed as Table 1.

Determination of the Similarity Coefficient and Similarity Material

Similarity criteria are essential in a physical model experiment, and the second theorem of similarity deduced by the dimensional analysis method is a widely adopted similarity criterion in physical model experiments (Li et al., 1996). The second theorem of similarity was adopted in this study. Another important parameter in the physical model experiment is the similarity coefficient C, which is defined by Eq. (1), where D_o is the quantity in the original model and D_s is the quantity in the scale model; they must be in the same unit.

$$C = \frac{D_o}{D_s} \tag{1}$$

$$\frac{C_\sigma}{C_L C\rho} = 1 \tag{2}$$

In this experiment, the scale model meets the similar criterion Eq. (2) according to the deduction of the second theorem of similarity. Thus, the basic geometry similarity coefficient C_L was set to 50, and the weight similarity coefficient C_ρ was set to 1. The stress similarity coefficient can then be determined by the second theorem of similarity, $C\sigma = 50$, where the stress quantity includes the elastic modulus and stress.

According to the geological investigation results of the Shuguang No. 6 section (Fig. 1), Quaternary gravel and moderately weathered sandstone are the main stratum types. Clay, sand, water, and Vaseline were adopted as the raw materials to make quaternary gravel and moderately weathered sandstone similar materials. We assumed that the material properties used to pave the subgrade were identical to quaternary gravel to simplify the experimental process. The mechanical difference of quaternary gravel and moderately weathered sandstone was obtained by adjusting the mix proportion

parameters. The parameters include the clay-sand ratio (m_c：m_s), water content ω, density ρ, and Vaseline content.

Similar materials of Quaternary gravel and moderately weathered gravel are made from clay and sand with different clay-sand ratios (m_c：m_s) and water contents (ω). A certain amount of Vaseline was added to increase the material strength. By a series of trial mixing experiments and strength tests of the samples, the mix proportions of similar materials are listed in Table 2. The original elastic modulus and density were obtained from the *Geotechnical Investigation Report of the Urumchi East Belt Expressway* (Transportation infrastructures administration of the Xinjiang 2017)

Physical Model System

Configuration and Dimension of the Physical Model Box

According to the strata condition of Shuguang No. 6 (Fig. 1), the thickness of the highly weathered sandstone strata is too thinner compared with other strata, it was omitted in the numerical model and physical model for the convenience of the analysis. A simplified strata model was established as Fig. 3. The dimensions of the strata model in reality and scaled mode are listed in Table 3.

As shown in Fig. 4, the model box's front and back sides were closed with 12 mm thick transparent organic tempered glass, and round steels supported the top and bottom sides of two organic tempered glass plates. The box's left and right sides were equipped with clamping slots that plank and inserted to close the box layer by layer as the similar material builds up. A semicircular hole was cut in the center of the front tempered glass plate to facilitate the extraction of pneumatic capsules buried in the soil to simulate the mining process.

In the experiment, pneumatic capsules were buried in the model box to simulate the mined-out space. The dimension of a Pneumatic capsule was 22 cm×11 cm×11 cm. There were five cases in the

model experiment; under different cases, the angle and height of the mined-out space shaped by pneumatic capsules were different. When similar material was filled into the model box, the height and the inclined angle of the pneumatic capsules were adjusted with the assistance of two planks. The dimensions of the supporting plank were 22 cm×11 cm×11 cm.

After the soil was filled to the elevation of the ground surface (190 cm) and compacted to the required density, the model was kept static for 10 days to simulate the consolidation process of natural strata. Then, the pneumatic capsule can be removed to simulate the mining process. The plank covering the exterior of the semicircle hole should be detached first to remove the pneumatic capsule. The pneumatic capsule was removed layer by layer from top to bottom by a clamp. Fig. 5 shows a scene of the mining simulation. Then, the subgrade could be quickly paved to the top of the model box. Meanwhile, the subgrade surface could be compacted and lightly leveled by a rubber hammer.

The Layout of Settlement Monitoring System

The strata settlement data in the experiment were obtained by dial gauges connected with the multipoint displacement measure embedded in the model box. There were 20 monitoring points (MPs) in the model (Fig. 6). The monitoring point arrangement and numbering are displayed in Eq. (3), where each element in the matrix represents a monitoring point. The first subscript of an element denotes its horizontal location: 1 means on the subgrade surface, 2 means on the subgrade bottom, 3 means on stratum 1, and 4 means on stratum 2. The second subscript signified the vertical location of this element, and all monitoring points with the same vertical make up a monitoring line (ML). Each ML consisted of a multipoint displacement measure and a surface dial gauge. The monitoring plane was located at the width center, parallel to the organic tempered glass plates. ML3 was positioned at the

model box's length center, which was also collinear with the centerline of the mined-out space floor.

$$\mathbf{M}=\begin{bmatrix} MP_{1-1} & MP_{1-2} & MP_{1-3} & MP_{1-4} & MP_{1-5} \\ MP_{2-1} & MP_{2-2} & MP_{2-3} & MP_{2-4} & MP_{2-5} \\ MP_{3-1} & MP_{3-2} & MP_{3-3} & MP_{3-4} & MP_{3-5} \\ MP_{4-1} & MP_{4-2} & MP_{4-3} & MP_{4-4} & MP_{4-5} \end{bmatrix} \tag{3}$$

Three layers of color sand were paved at the bottom of the subgrade, stratum 1 and stratum 2, to assist the internal settlement monitor of multipoint displacement measures, and the thickness of the color sand was 5 mm. The sand color was red, green, and purple in sequence from top to bottom (Ren et al., 2010).

Install dial gauges and Data reading

Two strong square section steels were stably placed on the top of the model box to fix the magnetic pedestals as Fig. 4. Dial gauges were then fixed on the magnetic pedestals. There were 20 dial gauges in total; 15 were connected with internal monitoring points on multipoint displacement measures by fishing threads, and the other 5 were set on the subgrade surface directly as Fig. 6. Each dial gauge was marked by a label in Eq. (3) to prevent data recording confusion

After the dial gauges are fixed and connected with the monitoring points correctly, record the dial gauge's initial data. Read the dial gauge data every 12 hours. Meanwhile, the location change of the colored sand layer was measured with a digital photographic system. The duration of data reading was 20 days. In this study, the settlement values analyzed were the stable settlement at the last recording. The settlement change with time was not discussed.

Physical Model Experiment Phenomenon

Settlement comparison between monitoring layers

Make the horizontal distance of a monitoring point to ML3 as the abscissa, right side (ML4, ML5) as the positive direction, left side (ML1, ML2) as negative direction; and the corresponding settlement value of each monitoring point as ordinate. According to the experimental case, connect the settlement value of monitoring points in Eq. (3) in the same row. The settlement curves of the mining height group cases and mining angle cases are exhibited in Figs. 7 and 8.

In Figs. 7 and 8, except for stratum 2 of case H20A65, from ML1 to ML4, the settlement increased gradually in the same horizontal layer and experimental case. The maximum and minimum settlements of each stratum were located at ML4 and ML1, respectively. From Fig. 9, ML4 was the closest monitoring line to the midpoint of the mined-out space roof, and ML1 was the farthest monitoring line. Thus, it can be deduced that the maximum settlement always occurred above the middle of the mined-out space roof. In the same horizontal monitoring layer, as the horizontal distance to the middle of the mined-out space roof increases, the settlement decreases.

Since the maximum settlement always occurred at ML4, the settlement decreased as the distance to ML4 increased. The shape of the horizontal monitoring layer settlements connecting lines was similar to an inverted funnel. Furthermore, as the mining height increased, the diameter and depth of the funnel increased. In contrast, as the mining angle increased, the diameter and depth of the funnel decreased slightly. Therefore, it could be concluded that the influence region of the strata overlying mined-out space increased as the mining height increased but decreased as the mining angle increased. The settlement lines of each group in the mining angle group were more concentrated than those in the

mining height group (Fig. 8), which implied that the effect of mining height was more striking than that of mining angle.

Settlement comparison between cases

The monitoring line's horizontal location was set as the abscissa, and the initial coordinate of monitoring point $M_{1\text{-}1}$ was chosen as the original point (0, 0). The settlement value was magnified 50 times and then added to the initial vertical coordinate of the monitoring point, and the initial monitoring points were drawn. Furthermore, the maximum settlement of each stratum was marked with its value. As a result, the settlement graphs of the mining height group and mining angle group experimenting cases are illustrated in Figs. 10 and 11.

The maximum settlement of each monitoring layer was extracted and grouped by experimenting with bar charts, and the changing trend of the maximum settlement is shown in Figs. 12 and 13. From the subgrade surface to stratum 2, the increasing rate of each case layer by layer is listed in Table 4.

By comparing the settlement layer by layer, as shown in Figs. 12 and 13, the lower stratum's settlement was larger than that of the upper stratum. The variation in the settlement mining angle group was not as steep as the mining height group, not only among the strata in the same case but also among the cases. There was no protruding case, such as case H30A75, which experienced more severe settlement than the other cases.

It is apparent from Figs. 7 and 8, Figs. 10 and 11 that the lower monitoring point's settlement is larger than the upper monitoring point at the same ML in all experimental cases. The settlement of the four monitoring layers increased gradually from top to bottom. The increasing rate of maximum settlement listed in Table 4 showed that the settlements at the surface and bottom of the subgrade were

nearly identical. Thus, the surface and bottom of the subgrade deformed together. Furthermore, as the mining height increases, the same horizontal layer increasing rate of the settlement increases among each experimental case in the mining height group. In cases, H10A75 and H20A75, each layer's settlement difference was uniform (the increasing rate was no more than 20%, and the largest settlement was just 0.579 mm). In case H30A75, the maximum increasing rate reached 61.8%, and the maximum settlements exceeded 1 mm at each layer, indicating stratum failure may occur in case H30A75. By contrast, the same horizontal layer increasing rate difference in the mining angle group between each case is mild. Moreover, the increasing rate of maximum settlement between different cases listed in Table 5 shows the same phenomenon as Table 4. Both signified that the subgrade and substrata settlement overlying acute inclined shallow mined-out areas are more sensitive to mining height changes than mining angles.

Numerical Simulation

There were only 20 monitoring points in the physical model experiment, and the experimental process of a physical model experiment is complex, time-consuming, and costly. A commonly used numerical method, the finite difference method used in geotechnical engineering by FLAC3D software, was adopted to analyze the strata settlement principle above the mined-out area deeply.

Numerical Model and Boundary Conditions

Numerical models with the same size as the actual simplified engineering prototype were established since there is no space limitation like the physical model. The physical model's size is scaled 1/50 according to similarity theory (the detailed dimension and strata configuration are shown in

Table 3 and Fig. 3). Five cases with the same mining parameters as the physical model experiment shown in Table 1 were calculated and analyzed. In the calculation, the model was generated with Brick elements in FLAC3D. The numerical model of case H30A75 is given in Fig. 14.

Boundary Condition and Material Property

The bottom of the model was constrained by fixed boundary conditions, in which no displacement or velocity was allowed; the boundary parallel to planes ZY and ZX was constrained by roller boundary conditions, which constrained the displacement and velocity in the normal direction of the boundary plane only. The top of the model was free without any displacement or velocity constraint.

There are two materials in the numerical model, intermediary weathered sandstone and quaternary gravel, similar to the physical model experiment. Moreover, the constitutive models included both Mohr-Coulomb models used in most geotechnical engineering. The subgrade material properties were the same as those of quaternary gravel, similar to the physical model experiment. The coal material was the same as intermediary weathered sandstone before coal excavation. In FLAC3D, the excavation process was modeled by defining the soil's material constitutive model that needed to be excavated to null (Li et al. 2021). The mechanical properties of the material related to the Mohr-Coulomb model obtained from the *Geotechnical Investigation Report of the Urumchi East Belt Expressway* (Transportation infrastructures administration of the Xinjiang 2017) are shown in Table 6.

Numerical Simulation Procedure

1. Establish the numerical model by FLAC3D according to the experimental case design in Table 1, which includes generating grids, defining material properties, and specifying boundary conditions.

2. Step to an equilibrium state and examine the model response to verify if the model is correct.
3. Initially, the displacement, velocity, and plastic zone caused by the geoequilibrium step are zero to eliminate the error resulting from geoequilibrium.
4. Define the material property of coal to null to simulate the mining process. Based on the most adverse load condition, full cross-section excavation was conducted without supporting measures to the excavated coal face.
5. Similarly, considering the most adverse load condition, the subgrade was paved with a total height of 5 m directly.
6. Obtain the contour of z-displacement (settlement) under each experimental case and contrast it with the physical model experiment settlement results. The highway subgrade and substrata's stability and settlement discipline overlying the mined-out area were analyzed based on the designed experimental case group.

Analysis of the Results

The settlement contours of the five cases analyzed are displayed in Fig. 15. According to these settlement contours, the lower strata settlement value is larger than the upper strata overlying the mined-out space layer by layer. Furthermore, the settlement contour is in the shape of an inverted funnel. The regions where maximum settlement occurred were located at the middle of the mined-out space roof, as ML3 was coincident with the floor of the mined-out space, and the middle of the roof was on the right side of the floor. The results were consistent with the maximum settlement distribution in the physical model experiments. In addition, the settlement of the subgrade surface and bottom was

nearly the same, suggesting the subgrade surface and bottom settlement were together. As seen from the settlement contour of mining height cases group (Fig. 15 b, d, e) and mining angle cases group (Fig. 15 a, b, c), respectively, as the mining height increases from 10 m to 30 m, the settlement value above the mined-out space increase gradually; as the mining angle increase from 65° to 85°, the settlement decrease gradually, however, the change gradient of settlement due to mining angle varying is not so steep as the settlement due to mining height varying. All of these phenomena were in agreement with the results obtained by physical model experiments.

Based on the settlement contours of all cases, the region with large settlements presented similar distribution characteristics. The large settlement region could be enclosed by two dashed lines, as shown in the settlement contours, which could be simplified and illustrated with Fig. 16. The right boundary extended from the mining inclining boundary to the ground surface parallel, similar to a slope; the left boundary extended from the lower-left corner to the ground surface at an angle. According to the Mohr strength criteria, the angle between the shear failure plane at any point in the material and maximum stress direction is [$\beta=45°-\varphi/2$] (He et al., 2002), where φ is the friction angle of the surrounding rock. Consequently, the direction of the maximum is vertical. By making the left boundary collinear with the potential shear failure line, the inclination angle can be illustrated as Fig. 16. However, this partitioning method is suitable for shallow mined-out areas only. For deep mined-out areas, shear failure is unlikely to extend to the ground surface according to Protodyakonov's pressure arch theory of collapse. (He et al., 2002)

Signify the mining width as w, mining height as h, overburden depth as d, θ as mining angle. The free slip volume with a unit length can be calculated with Eq. (4).

$$S = S_{DCEF} + S_{GAF} + S_{HGA}$$
$$= wd + \frac{(d+h)^2}{2\tan\theta} + \frac{(d+h)^2 \tan\left(45^o - \frac{\varphi}{2}\right)}{2} \quad (4)$$

From Eq. (4), the free slip volume is directly proportional to the mining height but is inversely proportional to the mining angle. The free slip volume is related to the overburden depth and mining width. Thus, it can be concluded that there were associations between mined-out area stability and overburden depth, and mining width. In this study, the overburden depth and mining width were fixed in the physical and numerical models. Therefore, the effects of overburden depth and mining angle were eliminated.

The area of the free surface in a unit length could be calculated with Eq. (5).

$$L = w + h / \sin\theta \quad (5)$$

The unit length values of free slip volume and free surface of the experimental cases could be calculated by Eqs. (4) and (5), respectively. The friction angle of φ *in* the surrounding rock was set as 30° to simplify the calculation. The calculation results are presented in Figs. 17 and 18.

As shown in Figs. 17 and 18, the free slip volume and free surface area were directly proportional to the mining height but inversely proportional to the mining angle. We substitute the values obtained in Figs. 17 and 18 into Eq. (6) to calculate the free slip volume and free surface gradients, respectively. According to the calculation results shown in Table 7, while the gradients of the free slip volume and free surface were larger than 70% for the mining height group, the gradient of the mining angle group was smaller, the gradient of the free slip volume was 32.7%, and the gradient of the free surface was only 5%. Therefore, compared with the mining angle, the stability of strata (including subgrade) overlying mined-out space is more sensitive to the change of mining height, which induces a more

significant change in the value of free slip volume and free surface. As the value of free slip volume and free surface is related to the settlement of strata overlying mined-out space, they could be the reference parameters to estimate the stability of strata and subgrade overlying acute inclined shallow mined-out space.

$$Gradient = \left| \frac{\text{Max. value - Min. value}}{\text{Min. value}} \right| \times 100\% \quad (6)$$

Table 1 Gradient of free slip volume and free surface of cases

	Mining height	Mining angle
Free slip volume	74.8%	32.7%
Free surface	70%	5%

Conclusion

The existence of an acute inclined shallow mined-out area has an evident effect on the stability of the overlying subgrade and strata. An acute inclined shallow mined-out area located in Urumqi, China, was traversed based on actual highway engineering. Two crucial factors (mining height and angle) that affect the strata deformation characteristics and failure mechanism due to acute inclined mine shallow mines were studied by physical model experiments and numerical simulation methods.

Five mining cases under varying mining heights and angles were implemented with physical model experiments and numerical simulations. They showed similar settlement features as the mining height and angle changes, and they were consistent. The following conclusions can be drawn from the experiments and numerical simulation results analysis:

(a). With increasing mining height, the subgrade and substrata settlement overlying acute

inclined shallow mined-out space increases accordingly. When the mining height was 30 m, the settlement was severely larger than that in the other experimental cases, and there may be a failure in the overlying strata and subgrade.

(b). With the increase in mining angle, the subgrade and substrata's settlement overlying mined-out space decreases slightly.

(c). In the strata overlying mined-out space, the lower layer's settlement is larger than that of the upper layer in the vertical direction. By contrast, the largest settlement is located above the midpoint of the mined-out space roof in the strata's horizontal direction, and as the horizontal distance to the midpoint of the mined-out roof increases, the settlement decreases. Thus, the settlement shape connecting lines were similar to an inverted funnel. Since highways are a form of long linear engineering, if the mined-out area underlying the highway was not properly treated, the nonuniform settlement is liable to occur at the highway mined-out section.

(d) According to the change rate and magnitude of the settlement under different experimental cases. The subgrade and substrata settlement overlying the mined-out space was more sensitive to the change in mining height than the mining angle.

(e) Define the influence region overlying the acute inclined shallow mined-out space as free slip volume, top, and left boundary of the mined-out space without the supporting area defined as free surface. The free slip volume and free surface calculation results of the experimental cases display a strong relationship between the settlement, free slip volume, and free surface. Therefore, the values of free slip volume and free surface could be reference parameters to evaluate the subgrade and substrata's stability overlying acute inclined shallow mined-out

areas.

Acknowledgements

This study was supported by the Xinjiang Uygur Autonomous Region Science and Technology Major Project (Grant No.: 2020A03003-7), Fundamental Research Project for Natural Science of Shaanxi Province (2021JM-180), Fundamental Research Funds for the Central Universities, CHD (Project for Leading Talents) (Grant No.: 300102211302), Science and Technology Program of Transportation Department of Xinjiang Uygur Autonomous Region (Grant No.: 2014-09), Tianshan Cedar Plan of Science and Technology Department of Xinjiang Uygur Autonomous Region (Grant No.: 2017XS13).

Conflict of Interest: The authors declare that they have no conflict of interest.

References

Álvarez-Vigil AE, González-Nicieza C, López Gayarre F, Álvarez-Fernández MI (2010) Forensic analysis of the evolution of damages to buildings constructed in a mining area (Part II) Engineering Failure Analysis 17:938-960 doi:https://doi.org/10.1016/j.engfailanal.2009.11.005

Bao W, Wang H, Lai H, Huang Y, Liang B, Ma Z (2021) Numerical stability analysis of superhigh-fill subgrade underlying acute inclined mined-out area with underground coal fire Environmental Earth Sciences 80:88 doi:10.1007/s12665-020-09346-z

Bell FG, de Bruyn IA (1999) Subsidence problems due to abandoned pillar workings in coal seams

Bulletin of Engineering Geology and the Environment 57:225-237 doi:10.1007/s100640050040

Cheng G, Chen C, Li L, Zhu W, Yang T, Dai F, Ren B (2018) Numerical modelling of strata movement at footwall induced by underground mining International Journal of Rock Mechanics and Mining Sciences 108:142-156 doi:https://doi.org/10.1016/j.ijrmms.2018.06.013

Cheng G, Chen C, Ma T, Liu H, Tang C (2017) A Case Study on the Strata Movement Mechanism and Surface Deformation Regulation in Chengchao Underground Iron Mine Rock Mechanics and Rock Engineering 50:1011-1032 doi:10.1007/s00603-016-1132-8

Cui X-M, Li C-Y, Hu Q-F, Miao X-X (2013) Prediction of surface subsidence due to underground mining based on the zenith angle International Journal of Rock Mechanics and Mining Sciences 60:246-252 doi:https://doi.org/10.1016/j.ijrmms.2012.12.036

Fang Y, Xu C, Cui G, Kenneally B (2016) Scale model test of highway tunnel construction underlying mined-out thin coal seam Tunnelling and Underground Space Technology 56:105-116 doi:https://doi.org/10.1016/j.tust.2016.03.007

Fathi Salmi E, Nazem M, Karakus M (2017) Numerical analysis of a large landslide induced by coal mining subsidence Engineering Geology 217:141-152 doi:https://doi.org/10.1016/j.enggeo.2016.12.021

Ghabraie B, Ren G, Barbato J, Smith JV (2017) A predictive methodology for multi-seam mining induced subsidence International Journal of Rock Mechanics and Mining Sciences 93:280-294 doi:https://doi.org/10.1016/j.ijrmms.2017.02.003

Guo W, Zhao G, Lou G, Wang S (2019) A New Method of Predicting the Height of the Fractured Water-Conducting Zone Due to High-Intensity Longwall Coal Mining in China Rock Mechanics and Rock Engineering 52:2789-2802 doi:10.1007/s00603-018-1567-1

He M, Jing H, Sun X (2002) Soft rock engineering mechanics. Science Press, Beijing

Holla L (1997) Ground movement due to longwall mining in high relief areas in New South Wales, Australia International Journal of Rock Mechanics and Mining Sciences 34:775-787 doi:https://doi.org/10.1016/S1365-1609(97)00004-1

Huayang D, Xugang L, Jiyan L, Yixin L, Yameng Z, Weinan D, Yinfei C (2010) Model study of deformation induced by fully mechanized caving below a thick loess layer International Journal of Rock Mechanics and Mining Sciences 47:1027-1033

doi:https://doi.org/10.1016/j.ijrmms.2010.06.005

Li, A., Dai, F., Liu, Y., Du, H.B., Jiang, R.C., 2021. Dynamic stability evaluation of underground cavern sidewalls against flexural toppling considering excavation-induced damage. Tunnelling and Underground Space Technology. 111, 103861.

Li D, Wang B, Lin Y (1996) Constructure model experiment. Science Press, Beijing

Marino G, Osouli A, Elgendy M, Karimpour M (2017) Utilization of Historical Subsidence Data for Prediction of Adverse Subsidence Conditions over Trona Mine 17:04016061 doi:doi:10.1061/(ASCE)GM.1943-5622.0000734

Meng Z, Shi X, Li G (2016) Deformation, failure and permeability of coal-bearing strata during longwall mining Engineering Geology 208:69-80 doi:https://doi.org/10.1016/j.enggeo.2016.04.029

Nie L, Wang H, Xu Y (2017) Application of the arctangent function model in the prediction of ground mining subsidence deformation: a case study from Fushun City, Liaoning Province, China Bulletin of Engineering Geology and the Environment 76:1383-1398 doi:10.1007/s10064-016-0913-3

O'Connor KM, Dowding CH (1992) Distinct element modeling and analysis of mining-induced subsidence Rock Mechanics and Rock Engineering 25:1-24 doi:10.1007/BF01041873

Ren W, Guo C, Peng Z, Wang Y (2010) Model experimental research on deformation and subsidence characteristics of ground and wall rock due to mining under thick overlying terrane International Journal of Rock Mechanics and Mining Sciences 47:614-624 doi:https://doi.org/10.1016/j.ijrmms.2009.12.012

Salmi EF, Nazem M, Karakus M (2017) The effect of rock mass gradual deterioration on the mechanism of post-mining subsidence over shallow abandoned coal mines International Journal of Rock Mechanics and Mining Sciences 91:59-71 doi:https://doi.org/10.1016/j.ijrmms.2016.11.012

Sepehri M, Apel DB, Hall RA (2017) Prediction of mining-induced surface subsidence and ground movements at a Canadian diamond mine using an elastoplastic finite element model International Journal of Rock Mechanics and Mining Sciences 100:73-82 doi:https://doi.org/10.1016/j.ijrmms.2017.10.006

Sheorey PR, Loui JP, Singh KB, Singh SK (2000) Ground subsidence observations and a modified

influence function method for complete subsidence prediction International Journal of Rock Mechanics and Mining Sciences 37:801-818 doi:https://doi.org/10.1016/S1365-1609(00)00023-X

Sui W, Hang Y, Ma L, Wu Z, Zhou Y, Long G, Wei L (2015) Interactions of overburden failure zones due to multiple-seam mining using longwall caving Bulletin of Engineering Geology and the Environment 74:1019-1035 doi:10.1007/s10064-014-0674-9

Sun Y, Zuo J, Karakus M, Wang J (2019a) Investigation of movement and damage of integral overburden during shallow coal seam mining International Journal of Rock Mechanics and Mining Sciences 117:63-75 doi:https://doi.org/10.1016/j.ijrmms.2019.03.019

Sun Y, Zuo J, Karakus M, Wen J (2019b) A Novel Method for Predicting Movement and Damage of Overburden Caused by Shallow Coal Mining Rock Mechanics and Rock Engineering doi:10.1007/s00603-019-01988-1

Transportation infrastructures administration of the Xinjiang (2017) geotechnical investigation report of Urumchi east belt expressway

Wang G, Wu M, Wang R, Xu H, Song X (2017) Height of the mining-induced fractured zone above a coal face Engineering Geology 216:140-152 doi:https://doi.org/10.1016/j.enggeo.2016.11.024

Wang Y, Yang J, Sun Z (2005) A handbook for reconnaissance and design & construction treatment of highway above mined-out area. China Communication Press, Beijing

Xia K et al. (2018) In situ monitoring and analysis of the mining-induced deep ground movement in a metal mine International Journal of Rock Mechanics and Mining Sciences 109:32-51 doi:https://doi.org/10.1016/j.ijrmms.2018.06.014

Xia K, Chen C, Liu X, Fu H, Pan Y, Deng Y (2016) Mining-induced ground movement in tectonic stress metal mines: a case study Bulletin of Engineering Geology and the Environment 75:1089-1115 doi:10.1007/s10064-016-0886-2

Xu Y, Wu K, Li L, Zhou D, Hu Z (2019) Ground cracks development and characteristics of strata movement under fast excavation: a case study at Bulianta coal mine, China Bulletin of Engineering Geology and the Environment 78:325-340 doi:10.1007/s10064-017-1047-y

Yao Q et al. (2017) Numerical investigation of the effects of coal seam dip angle on coal wall stability International Journal of Rock Mechanics and Mining Sciences 100:298-309 doi:https://doi.org/10.1016/j.ijrmms.2017.10.002

Zhang B, Zhang L, Yang H, Zhang Z, Tao J (2016) Subsidence prediction and susceptibility zonation for collapse above goaf with thick alluvial cover: a case study of the Yongcheng coalfield, Henan Province, China Bulletin of Engineering Geology and the Environment 75:1117-1132 doi:10.1007/s10064-015-0834-6

Zhang J, Wang j (2014) Similar simulation and practical research on the mining overburden roof strata "three-zones" height Journal of Mining & Safety Engineering 31:249-254 doi:10.13545/j.issn1673-3363.2014.02.014

Zhou D, Wu K, Li L, Diao X, Kong X (2016) A new methodology for studying the spreading process of mining subsidence in rock mass and alluvial soil: an example from the Huainan coal mine, China Bulletin of Engineering Geology and the Environment 75:1067-1087 doi:10.1007/s10064-016-0877-3

Figures

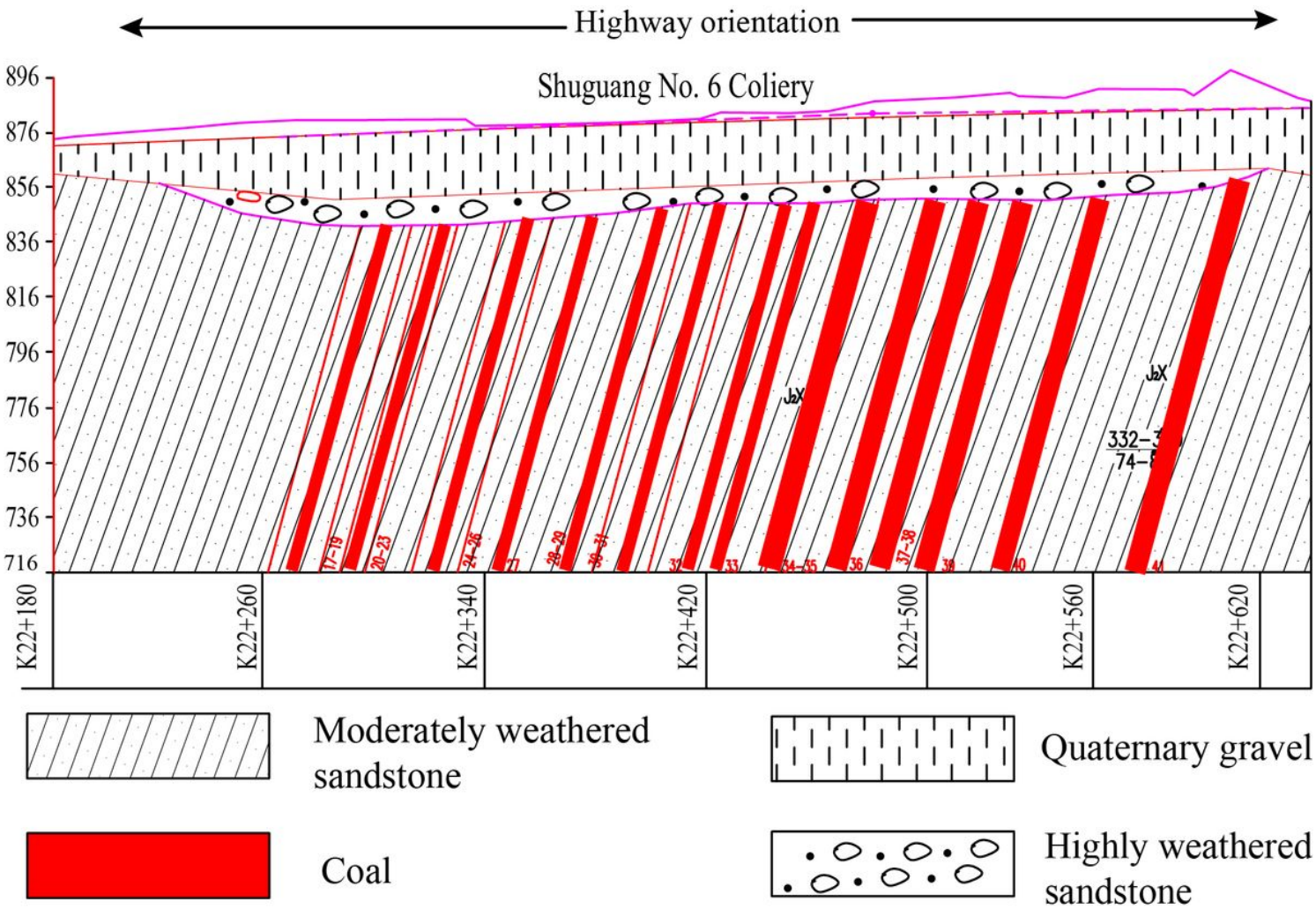

Figure 1

Longitudinal cross-section diagram of the prototypical mined-out area studied

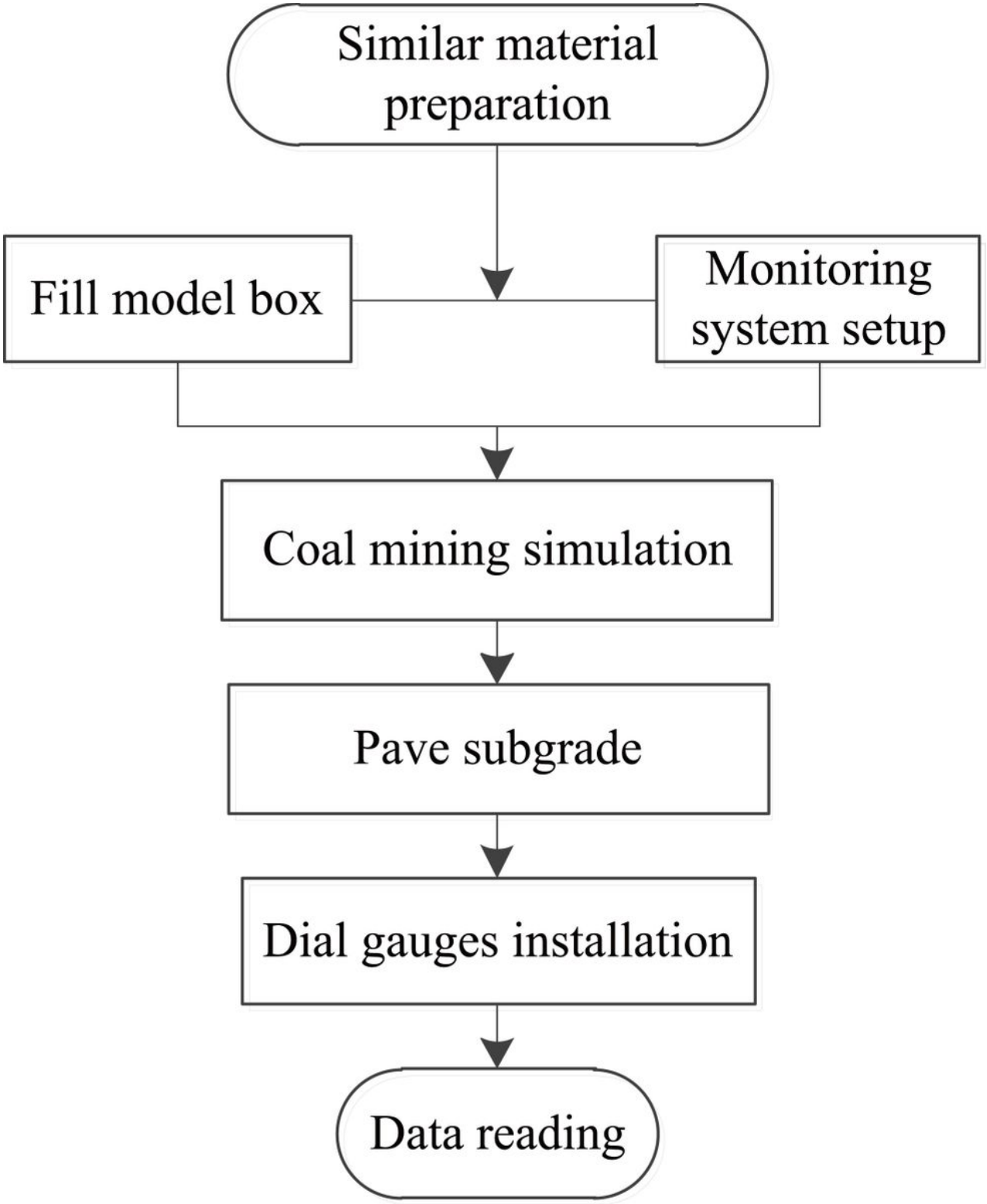

Figure 2

Physical model experiment flowchart

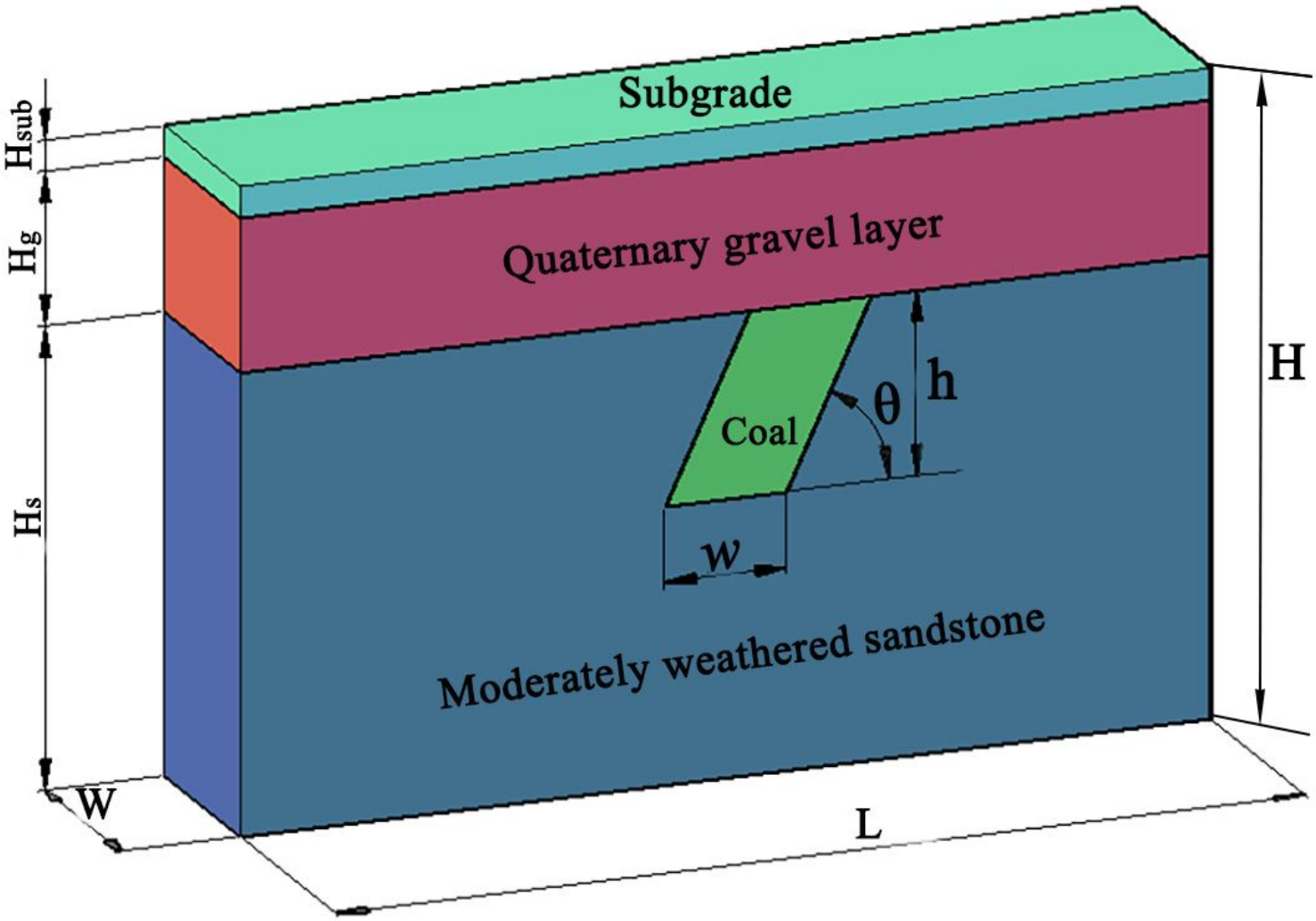

Figure 3

Configuration of the simplified strata model

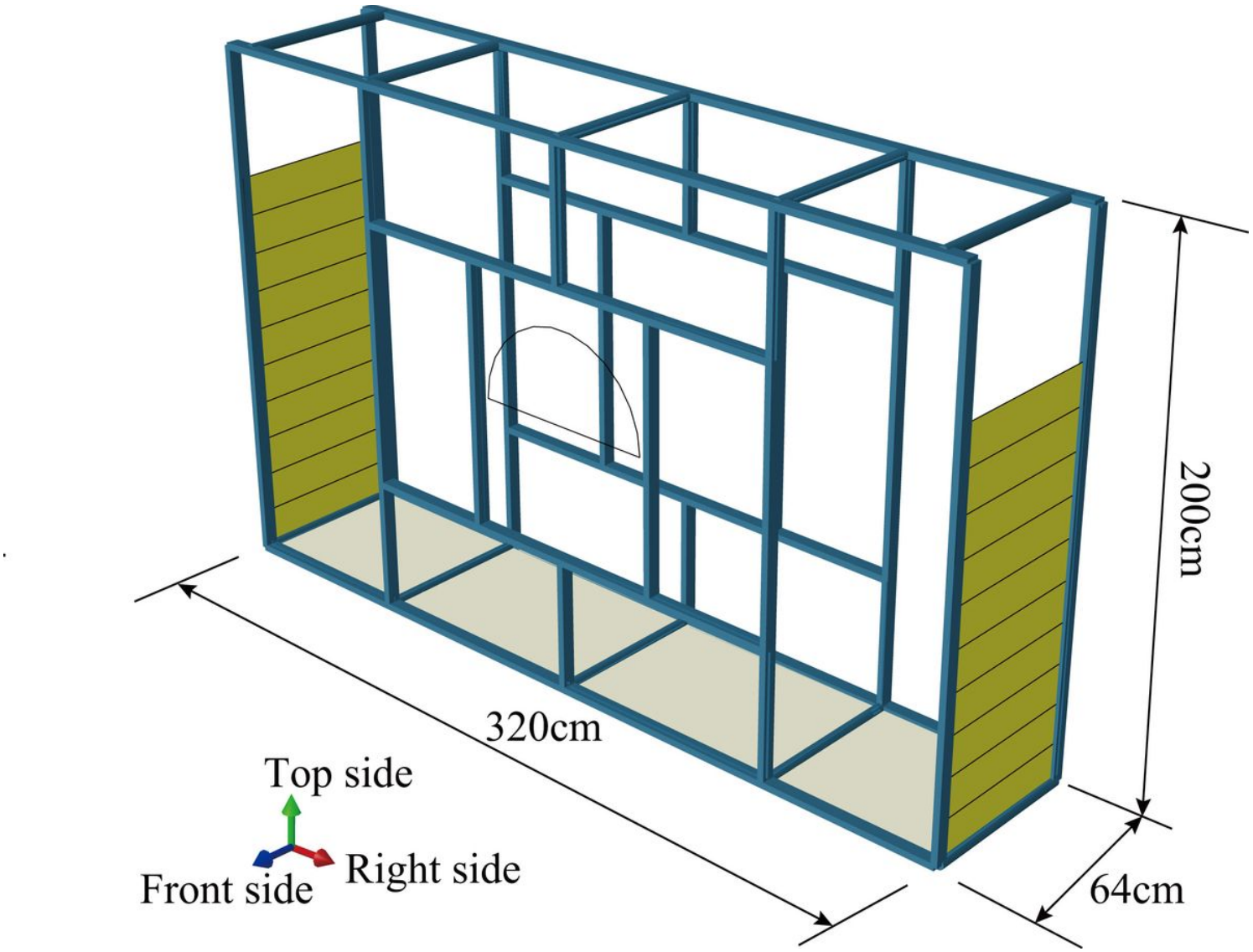

Figure 4

Configuration of the physical model box

Figure 5

Mining simulation by removing the plastic pneumatic capsule

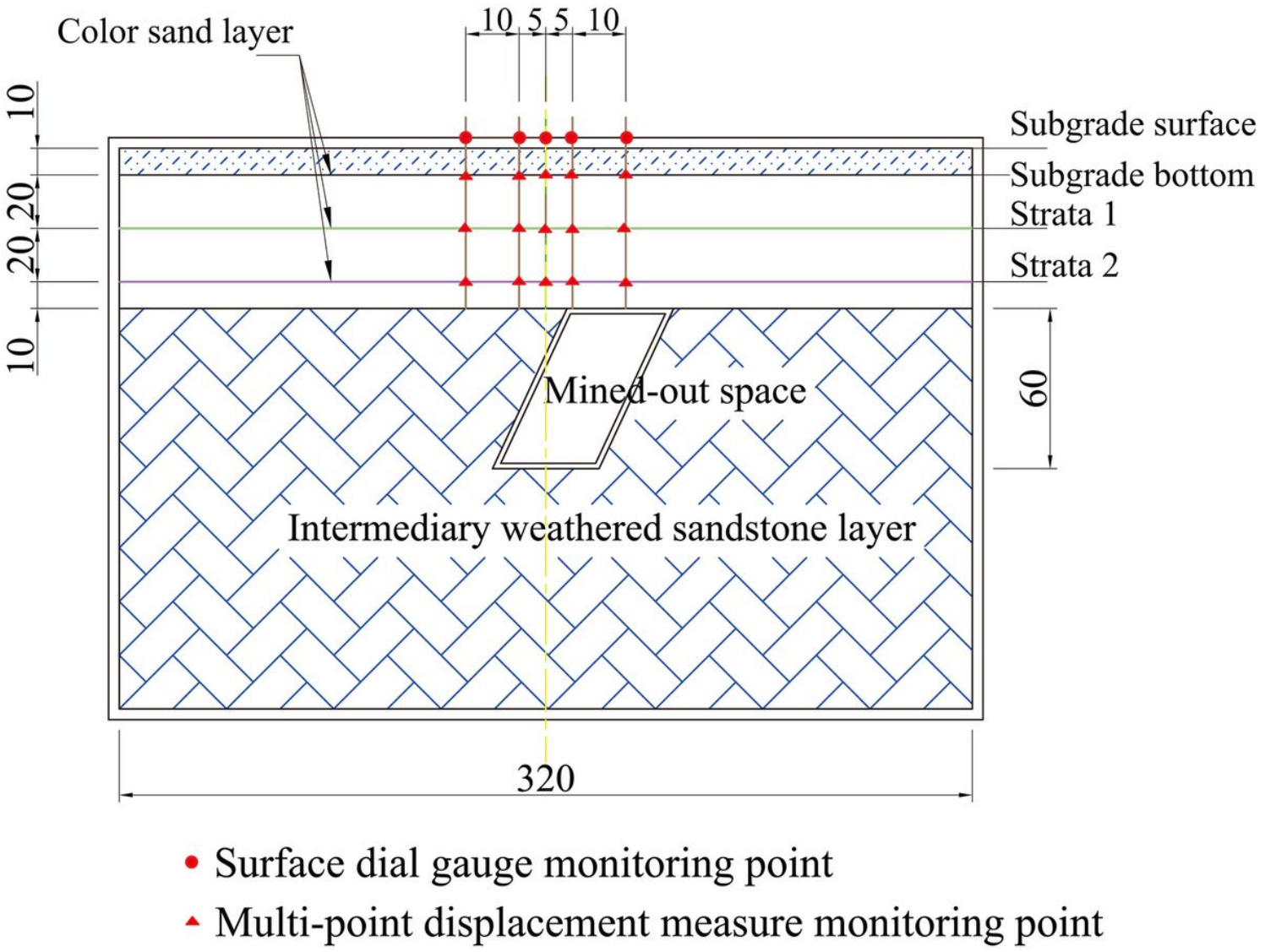

Figure 6

Arrangement of monitoring points and color sand (unit: cm)

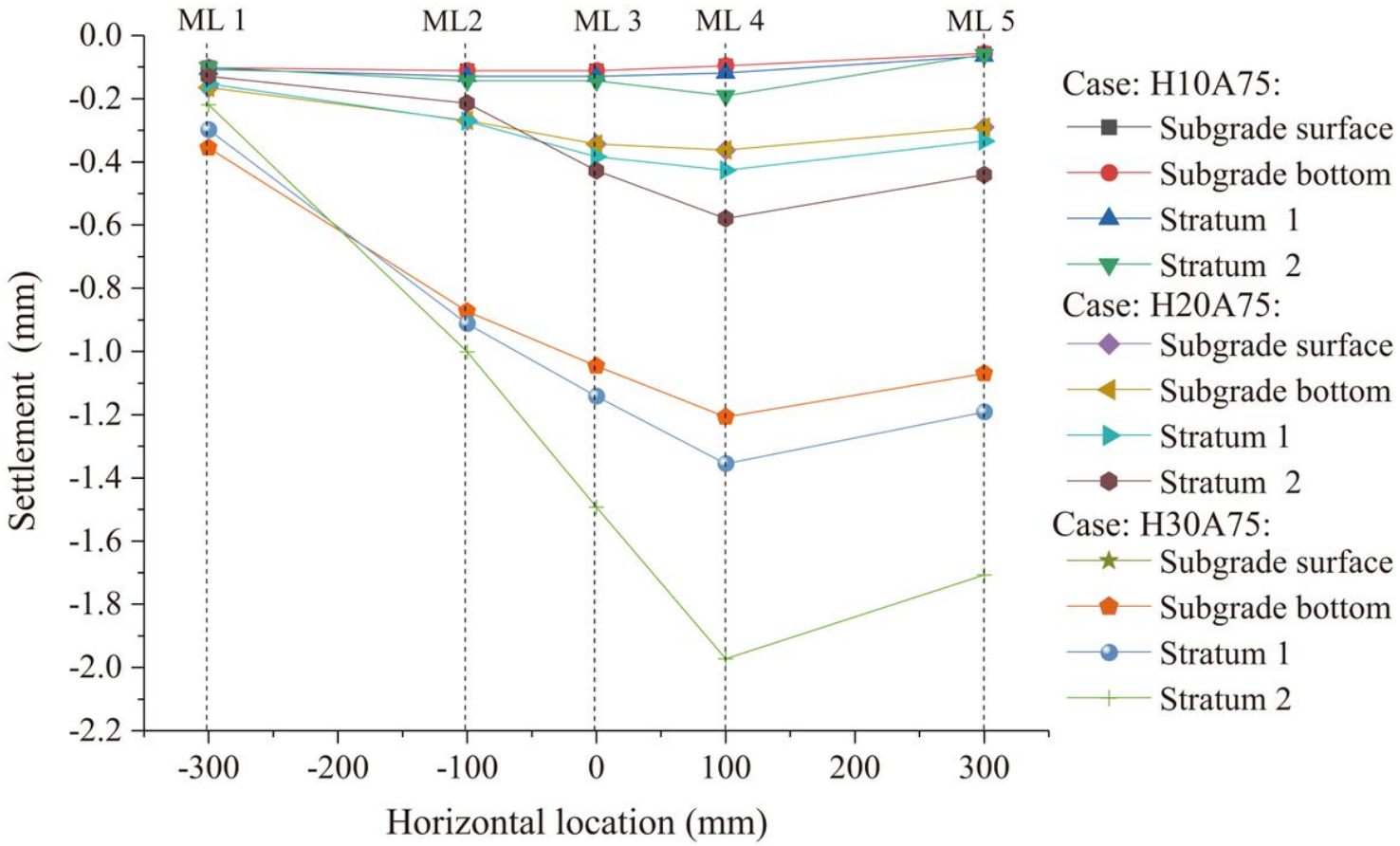

Figure 7

Settlements of the mining height group: mining heights are 10 m, 20 m, and 30 m, and mining angles are 75°

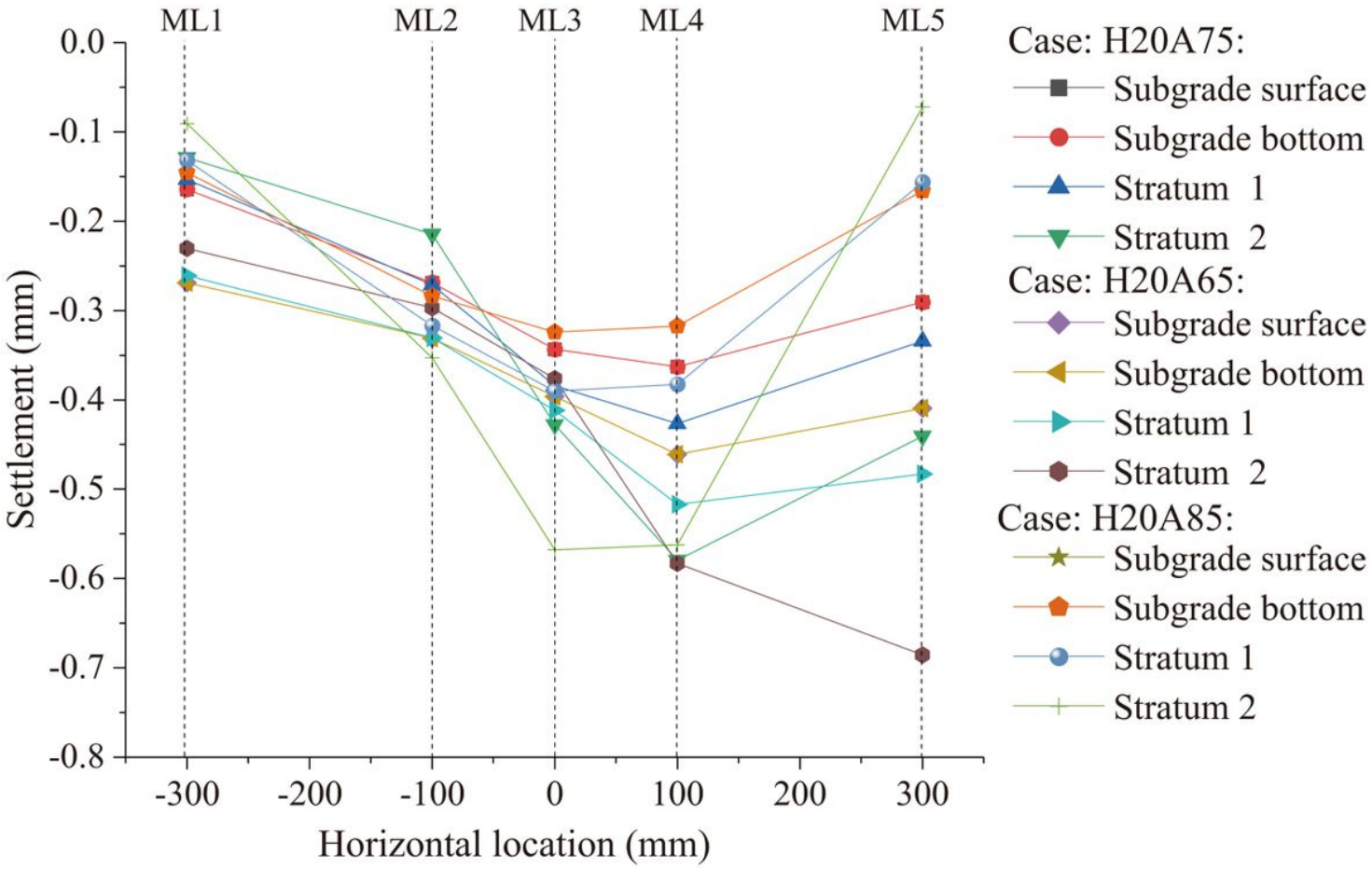

Figure 8

Settlements of the mining angle group: mining angles are 65°, 75°, and 85°, and mining heights are 20 m

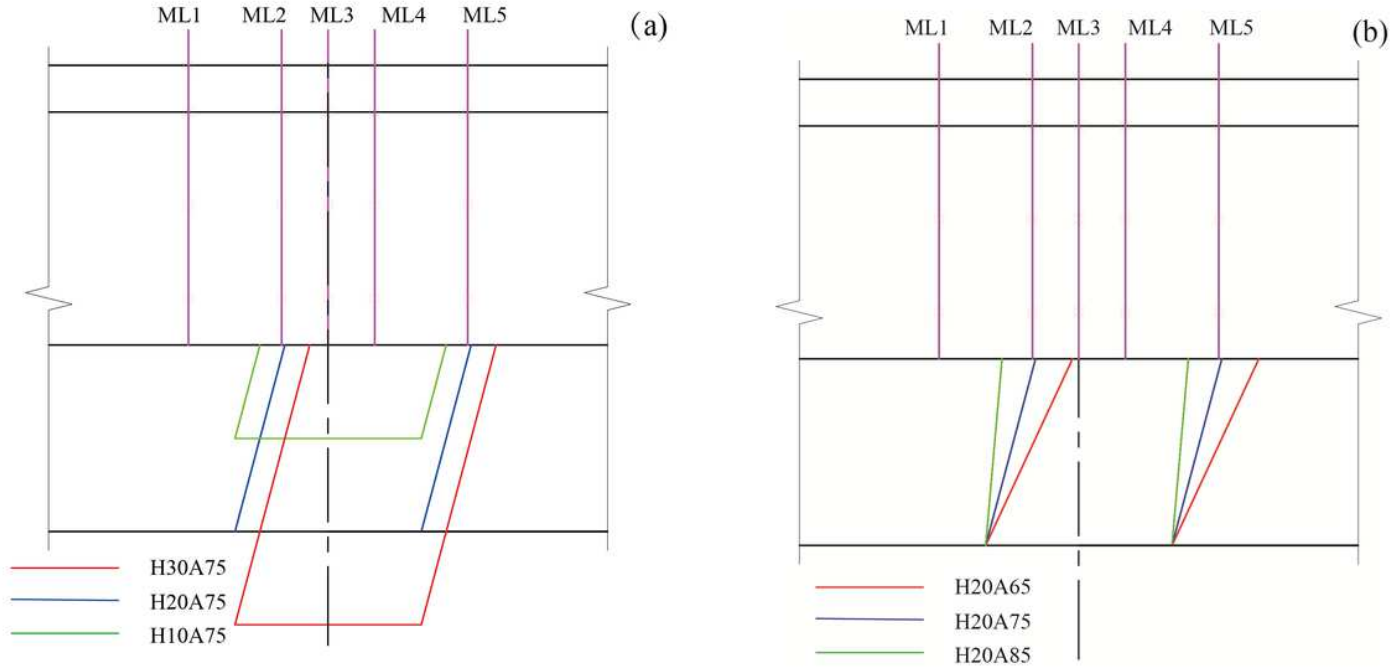

Figure 9

The relative position of the mined-out space: (a) Mining height group; (b) Mining angle group

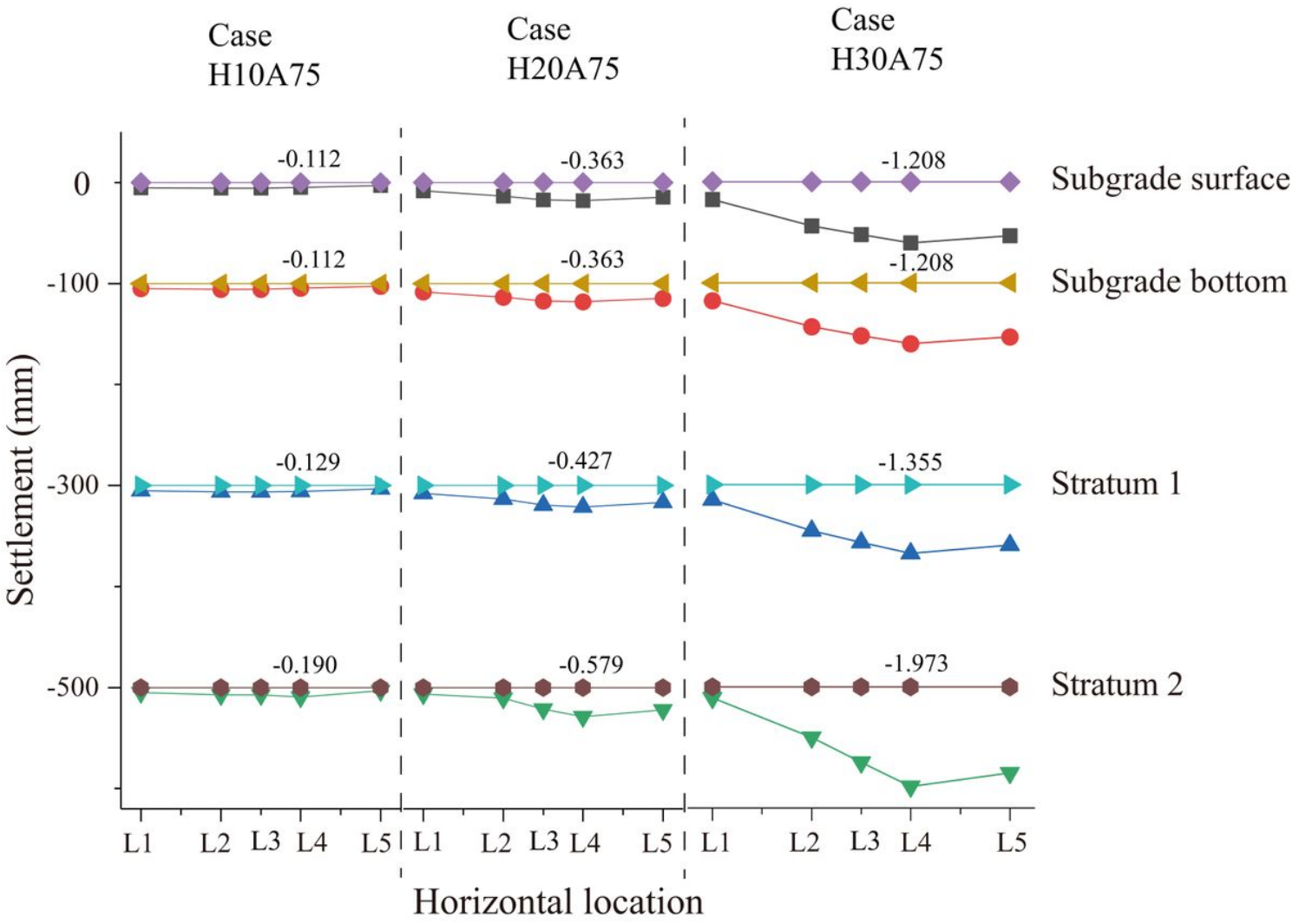

Figure 10

Strata settlement distribution and maximum settlement of the mining height group

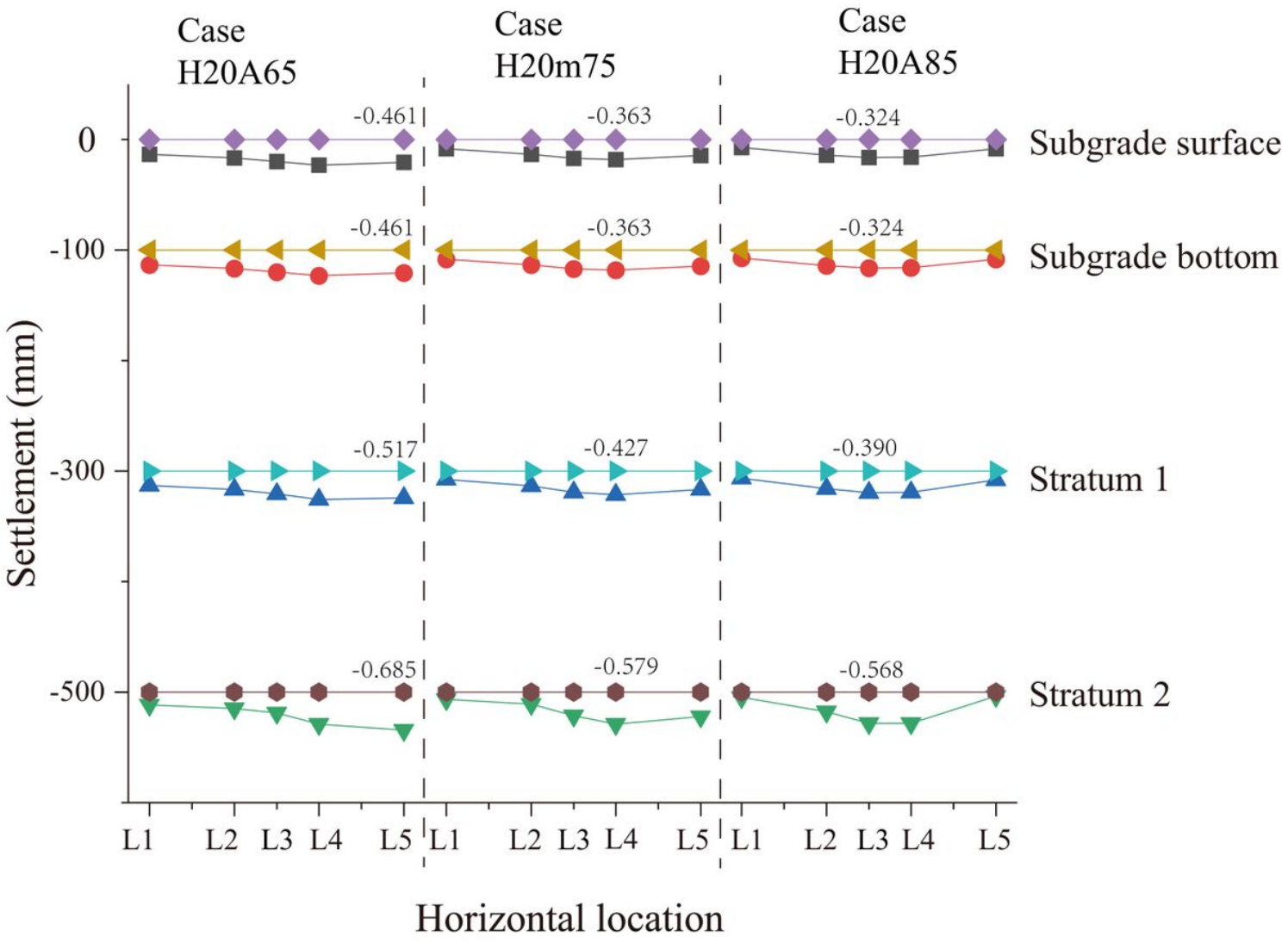

Figure 11

Strata settlement distribution and maximum settlement of the mining angle group

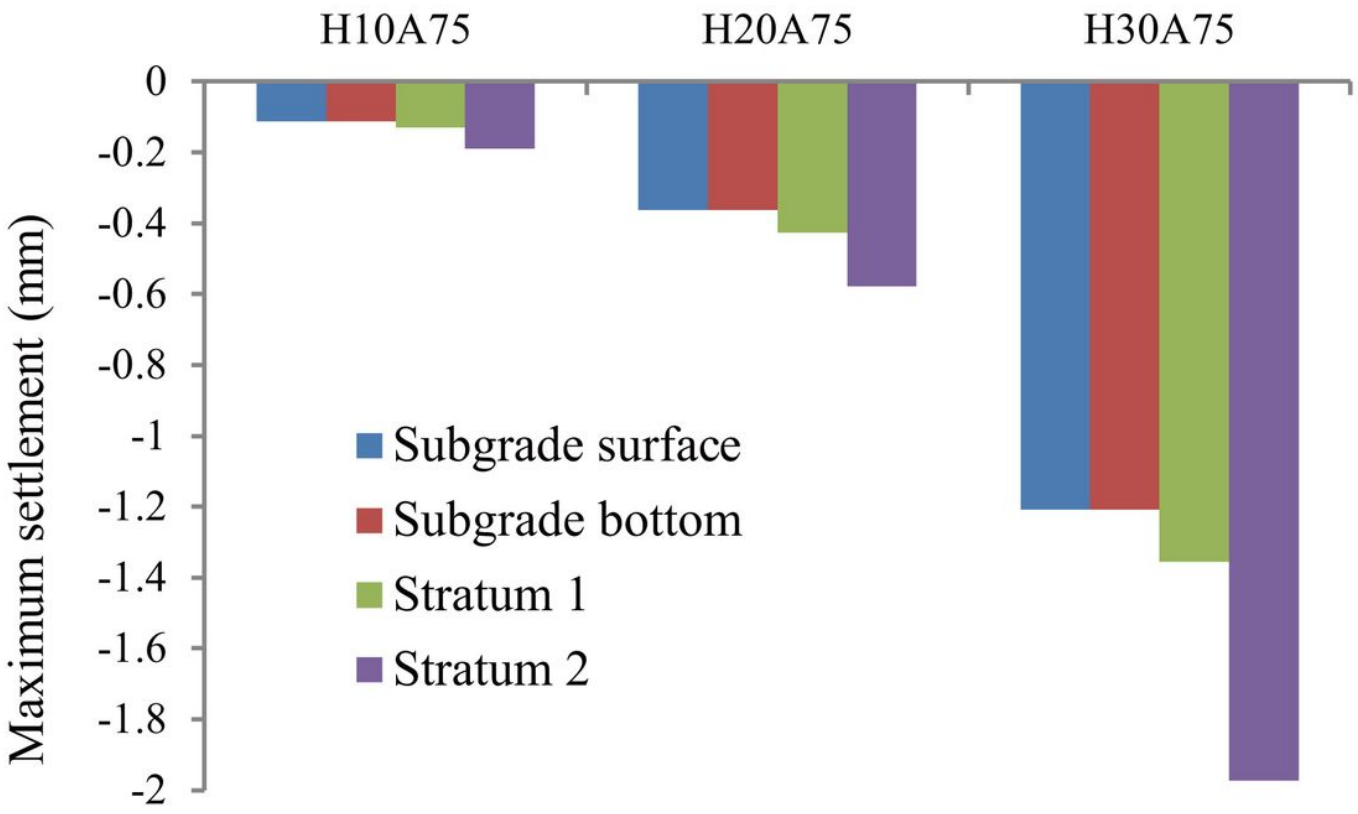

Figure 12

Maximum settlement of the mining height group

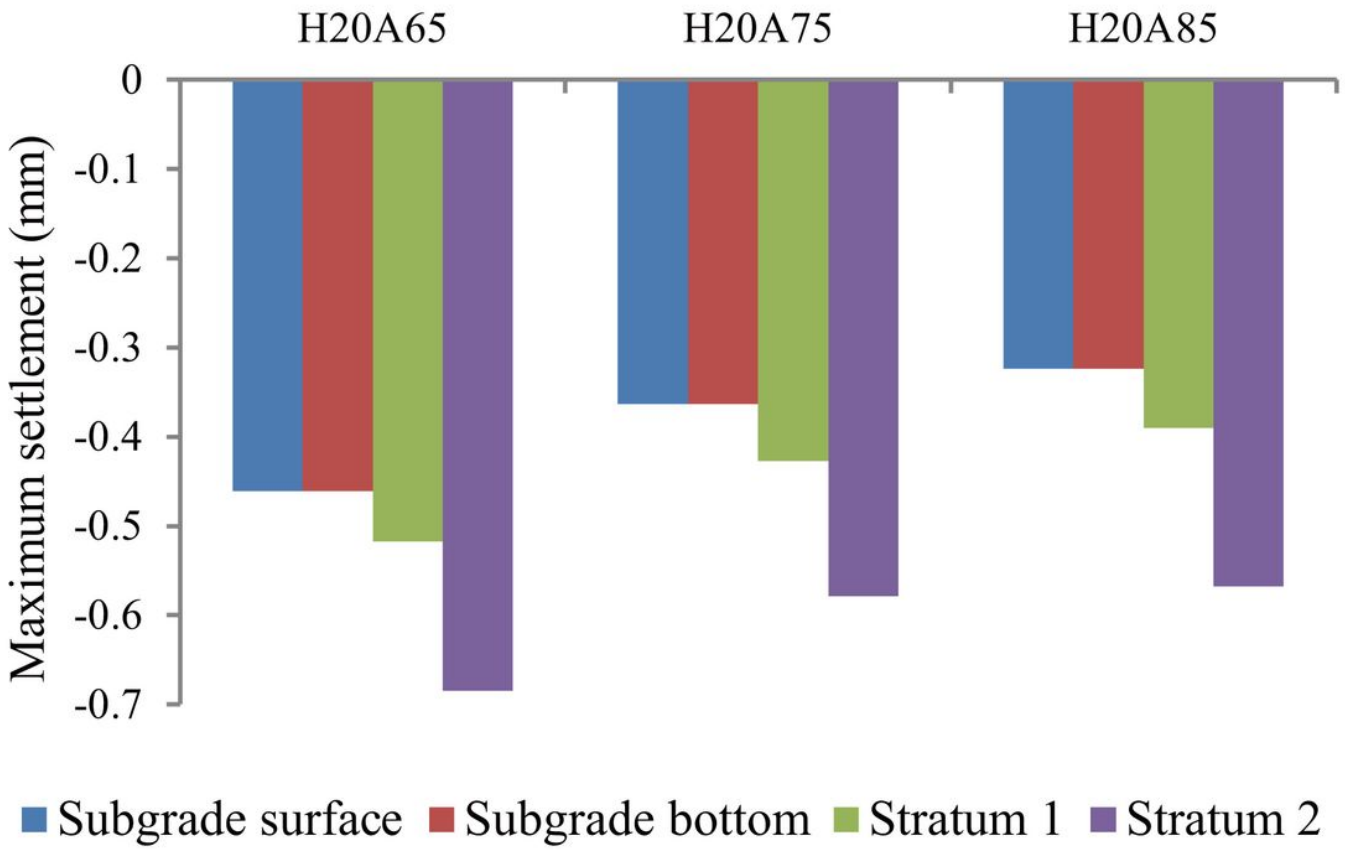

Figure 13

Maximum settlement of the mining angle group

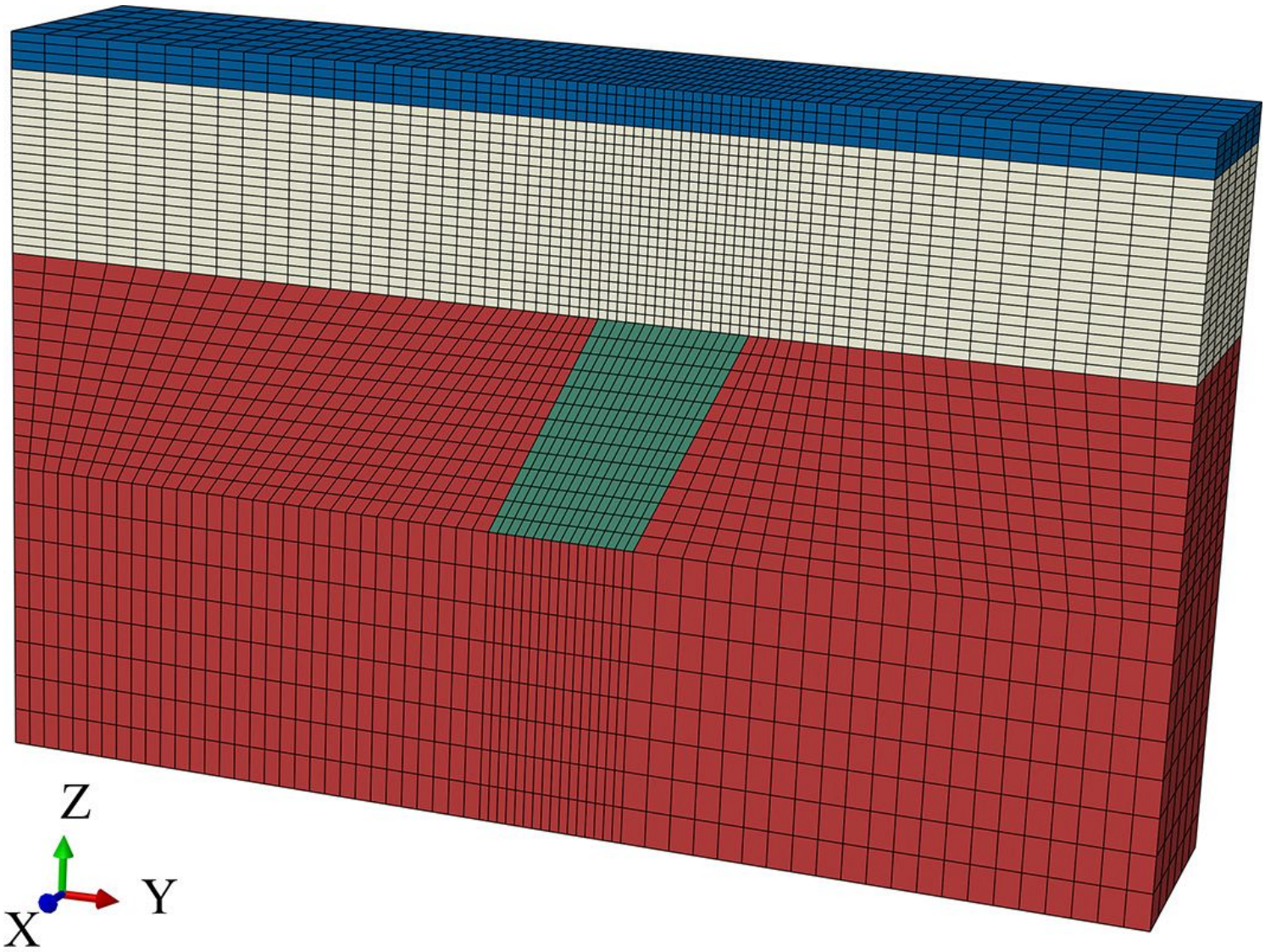

Figure 14

Numerical model of case H30A75 (mining height is 30 m, mining angle is 75°)

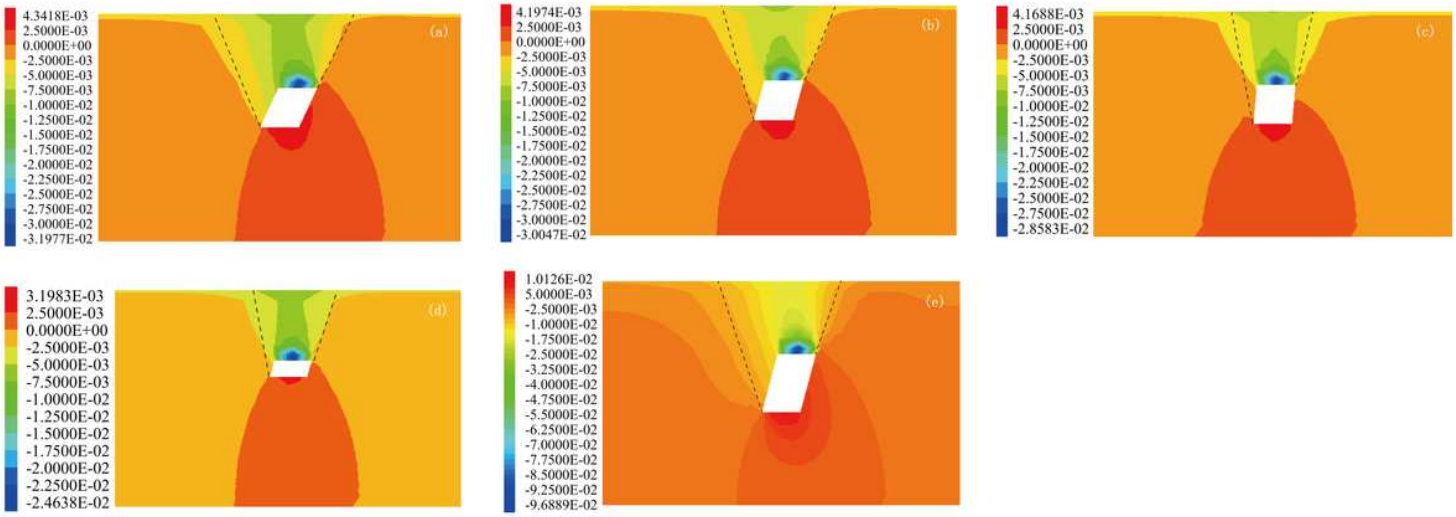

Figure 15

Settlement contours of all calculation cases: (a) H20A65; (a) H20A65; (b) H20A75; (c) H20A85; (d) H10A75; (e) H30A75 (settlement unit: m)

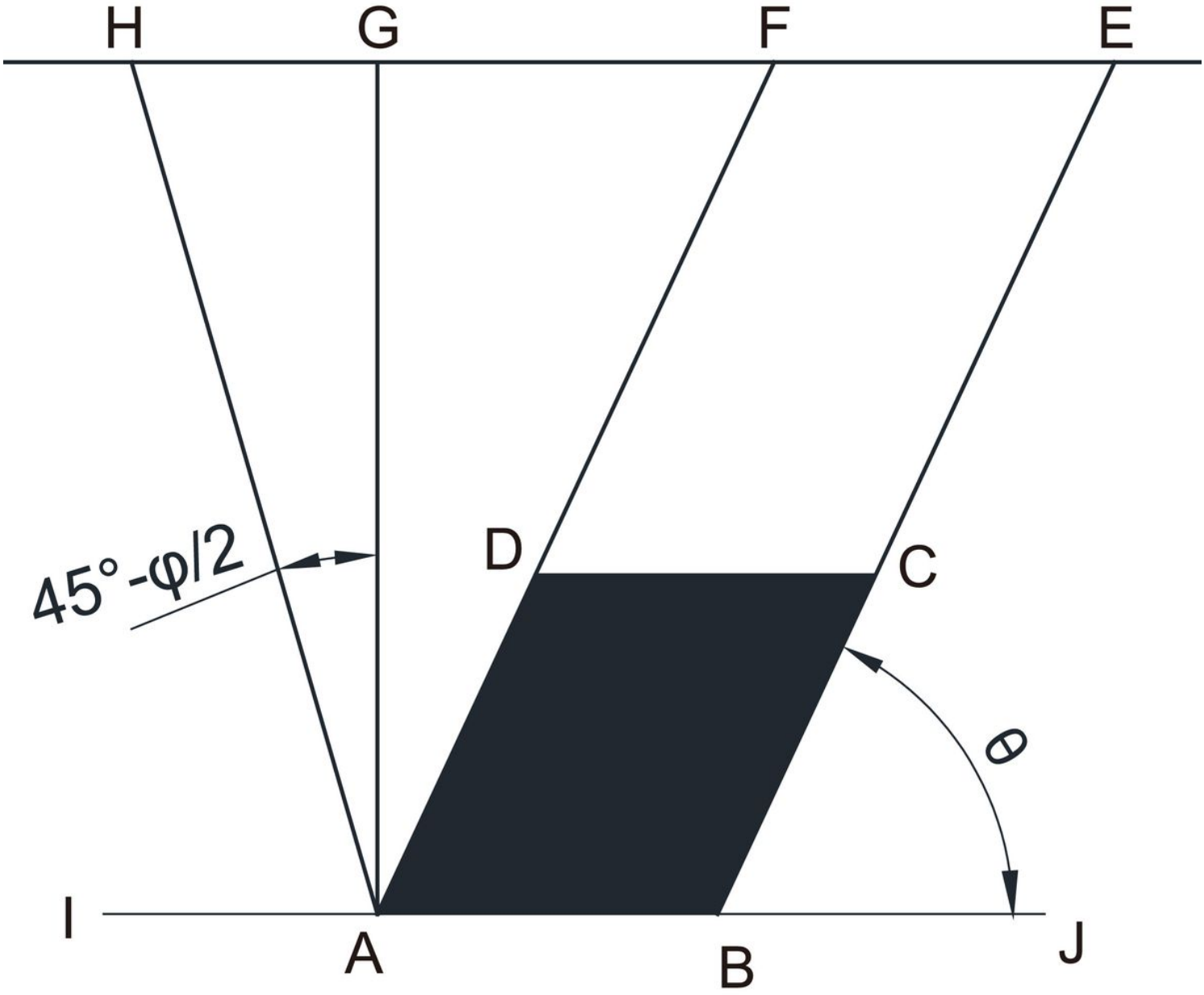

Figure 16

Diagram of mined-out space free surface and free slip volume

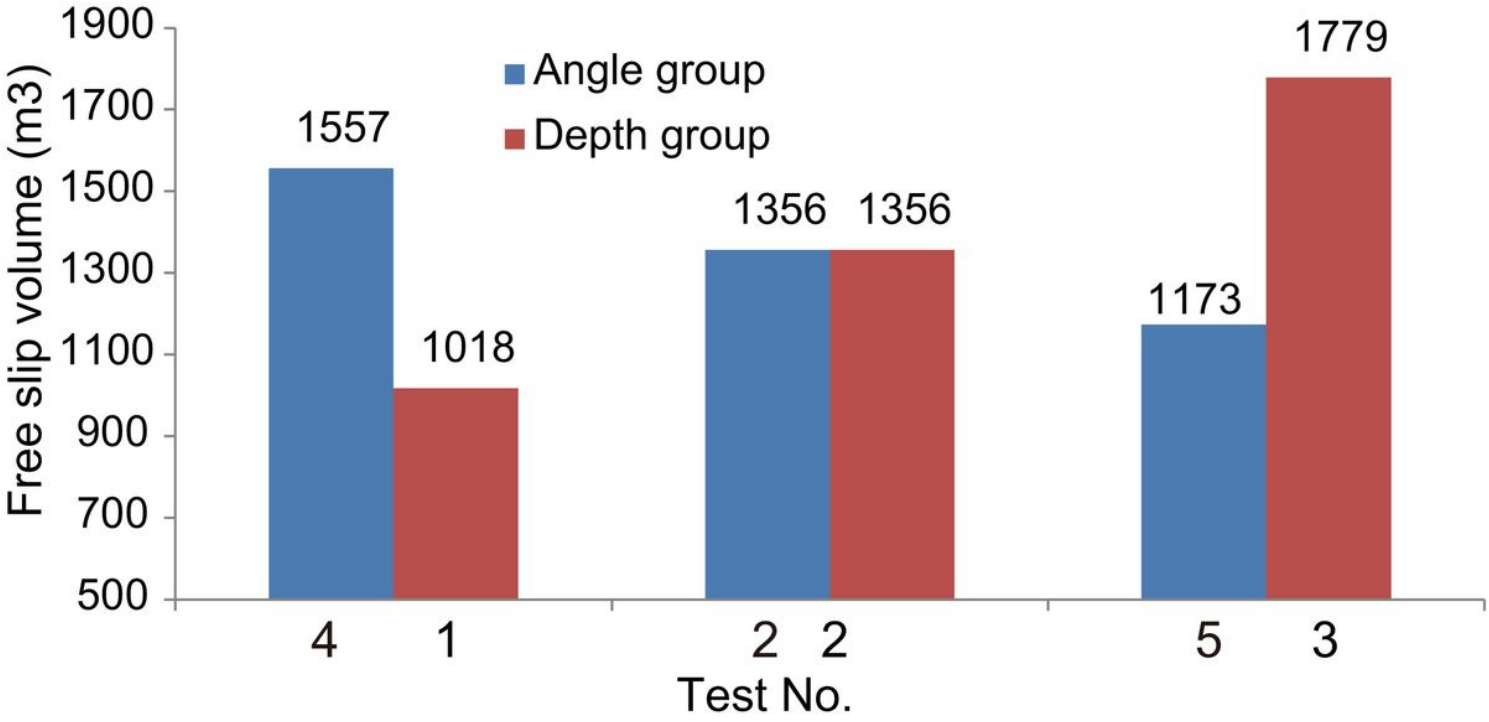

Figure 17

Free slip volume of all cases

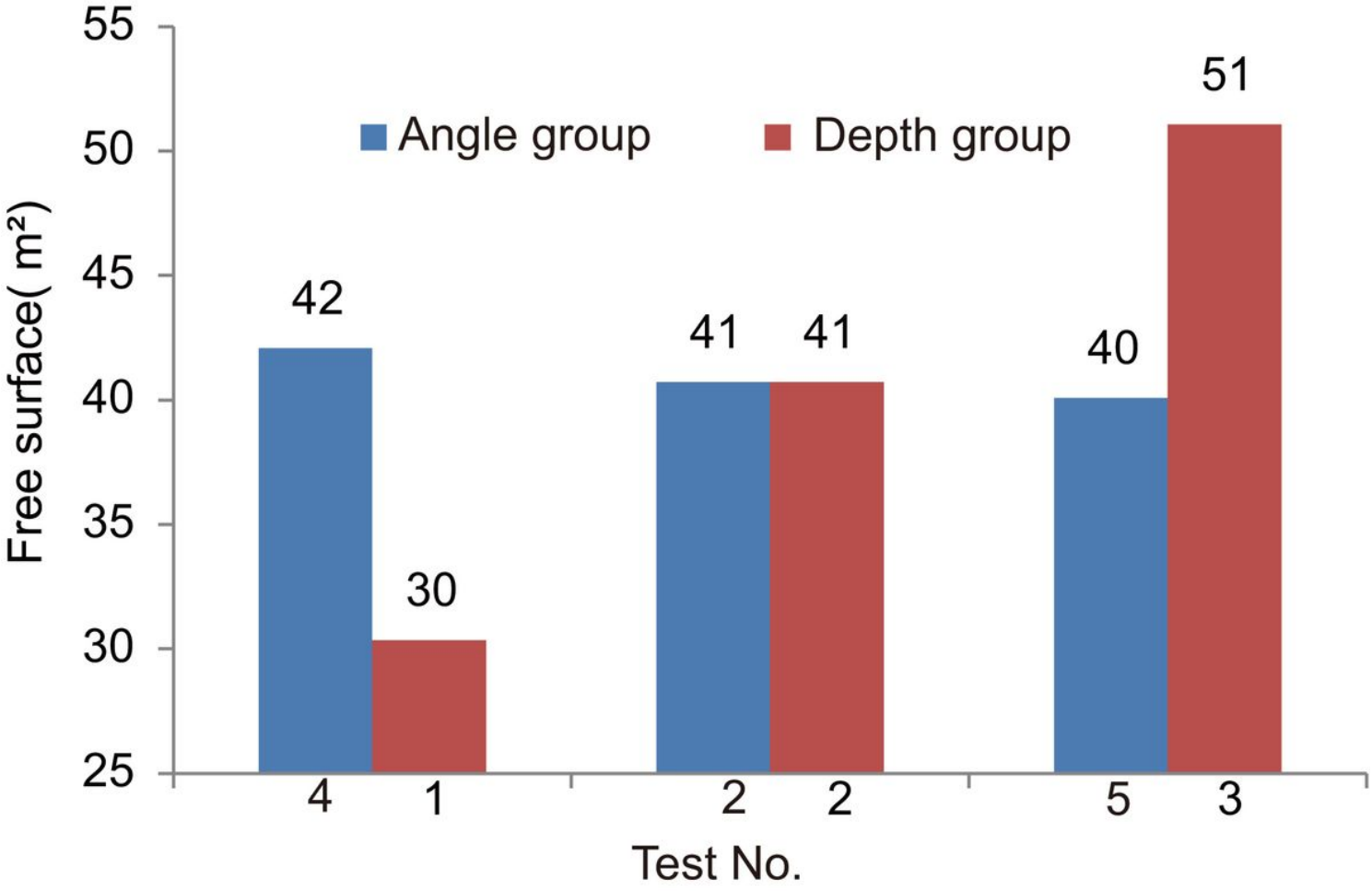

Figure 18

Free surface of all cases